Geological Survey
of Canada

CURRENT RESEARCH

2004-C5

Electrical conductivity mechanism of graphitic shale from the Astarte River formation, Piling Group, Baffin Island, Nunavut

S. Connell-Madore, P. Hunt, and J. Li

2004

Natural Resources Canada | Ressources naturelles Canada

Canada

106-03727/

©Her Majesty the Queen in Right of Canada 2004
ISSN 1701-4387
Catalogue No. M44-2004/C5E-PDF
ISBN 0-662-36979-3

Available in Canada from the
Geological Survey of Canada Bookstore website at:
http://gsc.nrcan.gc.ca/bookstore/ (Toll-free: 1-888-252-4301)

A copy of this publication is also available for reference by depository libraries across Canada through access to the Depository Services Program's website at http://dsp-psd.pwgsc.gc.ca

All requests for permission to reproduce this work, in whole or in part, for purposes of commercial use, resale, or redistribution shall be addressed to: Earth Sciences Sector Information Division, Room 402, 601 Booth Street, Ottawa, Ontario K1A 0E8.

Authors' addresses

S. Connell Madore *(sconnell@nrcan.gc.ca)*
P. Hunt *(phunt@nrcan.gc.ca)*
Geological Survey of Canada
601 Booth Street
Ottawa, Ontario K1A 0E8

J. Li *(jili@nrcan.gc.ca)*
Materials Technology Laboratory - CANMET
568 Booth Street
Ottawa, Ontario K1A 0G1

Publication approved by Mineral Resources Division

Original manuscript submitted: 2004-02-26
Final version approved for publication: 2004-03-25

Electrical conductivity mechanism of graphitic shale from the Astarte River formation, Piling Group, Baffin Island, Nunavut

S. Connell-Madore, P. Hunt, and J. Li

Connell-Madore, S., Hunt, P. and Li, J., 2004: Electrical conductivity mechanism of graphitic shale from the Astarte River formation, Piling Group, Baffin Island, Nunavut; Geological Survey of Canada, Current Research 2004-C5, 9 p.

Abstract: Textural examination using scanning electron microscope analysis, was carried out on four graphitic shale subsamples, from the Astarte River formation, Baffin Island, Nunavut. Electrical resistivity measurements previously made on these mineralized rocks indicate that they display weak to strong anisotropic characteristics (5:1 to 275:1), with low and high resistivities of 8–16 000 Ω•m and 390–40 000 Ω•m in the directions parallel and perpendicular to foliation, respectively. The purpose of this study was to determine the electrical conductivity mechanisms that resulted in these characteristics.

The results of this study suggest that well connected quartz grains form electrically insulating layers and result in the high electrical resistivities (3580 to more than 28 000 Ω•m) in the direction perpendicular to foliation. The low resistivity characteristics parallel to foliation are likely determined by moderately good pore-fluid connectivity. Scanning electron microscope analysis indicates that graphite also contributes to the low resistivity.

Résumé : À l'aide d'un microscope électronique à balayage, on a examiné en détail la texture de quatre sous-échantillons de shale graphitique de la formation d'Astarte River, dans l'île de Baffin (Nunavut). Des mesures antérieures de la résistivité électrique de ces roches minéralisées indiquent que ces roches présentent des valeurs d'anisotropie variant de faibles à fortes (de 5/1 à 275/1) et des valeur maximales et minimales de la résistivité électrique comprisent entre 8 et 16 000 Ω•m et entre 390 et 40 000 Ω•m, respectivement, dans les directions parallèle et perpendiculaire à la foliation. La présente étude avait comme objet de déterminer les mécanismes de la conductivité électrique auxquels il faut attribuer ces caractéristiques.

Les résultats indiquent que des grains de quartz ayant une bonne connectivité forment des couches agissant comme isolateurs électriques et engendrent des valeurs élevées de résistivité électrique (de 3580 à plus de 28 000 Ω•m) dans la direction perpendiculaire à la foliation. La faible résistivité électrique dans la direction parallèle à la foliation est vraisemblablement attribuable à une connectivité modérément bonne du fluide interstitiel. L'analyse au microscope électronique à balayage révèle que du graphite contribue également à la faible résistivité.

INTRODUCTION

Detailed textural examination using scanning electron microscope (SEM) analysis, secondary electron imaging (SEI), and backscatter electron (BSE) imaging, was carried out on four graphitic shale samples, from the Astarte River formation, Piling Group, Baffin Island. Electrical resistivity measurements previously made on these mineralized rocks (Scromeda-Perez and Connell-Madore, 2004) indicated that they display weak to strong anisotropic characteristics (5:1 to 275:1), with the low and high resistivities in the ranges of 8 to 16 000 Ω•m and 390 to 40 000 Ω•m in the directions parallel and perpendicular to foliation, respectively. The purpose of this study was to explain the reason for these characteristics by analyzing their electrical conductivity mechanism. The electrical resistivity and porosity data, previously obtained to assist this analysis, are summarized in Table 1. This study was intended to eventually assist in interpreting ground electromagnetic surveys which have been conducted in the area.

METHOD OF INVESTIGATION

The four samples, BAF-1, BAF-2, BAF-3, and BAF-AB, investigated in this study were supplied by A. Jones (GSC) and have previously been used for 3-D electrical resistivity measurements (Scromeda-Perez and Connell-Madore, 2004). Four specimens were cut off each of these samples for electrical resistivity measurements, porosity measurements, graphite thin-section analysis (Fig. 1), and scanning electron microscope analysis (Fig. 2–5). Four specimens (BAF-1x1, BAF-2x1, BAF-3x1, and BAF-ABx1) were prepared for SEM analysis.

The specimens used for the electrical measurements were previously cut into rectangular blocks (Scromeda-Perez and Connell-Madore, 2004), with one side parallel to foliation and the other two sides perpendicular to foliation. First, a detailed visual examination was performed on these specimens and key features recorded, as shown in the block diagrams (*see* Fig. 2–5). Since it was not possible to polish the rectangular blocks used for the electrical measurements, adjacent specimens were used for SEM analysis. These surfaces were mounted in epoxy, polished, and prepared for SEM analysis. This analysis included examination of sample mineralogy, texture, and fabric of the sulphide and other mineral grains that influence the flow of electrical currents through the rock. One set of four specimens were shipped to Vancouver Petrographics Ltd. (Vancouver, British Columbia) for polished thin-section preparation and graphite analysis (Fig. 1).

The SEM analysis was conducted at two separate laboratories: one at the Geological Survey of Canada (GSC) and the other at the Canada Centre for Mineral and Energy Technology (CANMET). A Leica/Cambridge S-360 SEM with an Oxford/Link eXL-II energy dispersive X-ray analyzer (EDS) was used for a portion of this analysis (GSC). Operating conditions for the SEM were generally 20 kV accelerating voltage at a 25 mm working distance with a 1 nA probe count. A Philips XL-30 SEM equipped with an Instrument ultra-thin window EDS was used also (CANMET). Operating conditions for this system were generally 20 kV accelerating voltage at 10 mm working distance. Backscattered electron and secondary electron images were produced as a result. A detailed description of SEM methods and procedures can be found elsewhere (Reed, 1997).

ANALYTICAL RESULTS AND INTERPRETATION

The mineralogy is essentially the same for each of the samples. Minerals identified under the SEM include quartz, muscovite, phlogopite, graphite, rutile, pyrite, pyrrhotite, and zircon. Titanite, sphalerite, chalcopyrite, and replacement montmorillonite were identified in sample BAF-AB only. Common recrystallized patches and lenses consisted of quartz, pyrite, microcline, muscovite, pyrrhotite, and chalcopyrite. Jarosite is a common weathering product except in sample BAF-AB. Not all minerals identified are shown in the SEM images in Figures 2 to 5. Evidence of sulphide remobilization has been detected in the axial planes of folds of this formation (Corrigan et al, 2001), and evidence of that is seen in sample BAF-B where pyrite veinlets are identified. Evidence of graphite remobilization has also been detected in sample BAF-1, where graphite lenses are concentrated in a fold nose. Graphite has been identified on polished thin sections with 0.5–4% concentrations in the samples.

Table 1. Summary of electrical resistivity (Scromeda-Perez and Connell-Madore, 2004) and porosity (Connell-Madore et al., 2004) data for Astarte River formation graphitic shale samples.

Sample number	Bulk electrical resistivity, ρ_i (Ω•m)			Anisotropy, λ	Effective porosity, ϕ_e (%)	Storage porosity, ϕ_s (%)	Connecting porosity, ϕ_c (%)
	α- direction	β-direction	γ-direction				
BAF-1	3580	13	82	275:1	14.22	12.87	1.35
BAF-2	2130	48	61	44:1	14.1	11.81	2.29
BAF-3	390	8	36	49:1	7.68	6.66	1.03
BAF-AB	>40 000	2500 to >16 000	2300 to >8000	5:1 to 12:1	4.19	2.72	1.47

α = Measurement made in the direction perpendicular to foliation.
β, γ = Measurement made in directions parallel with foliation.

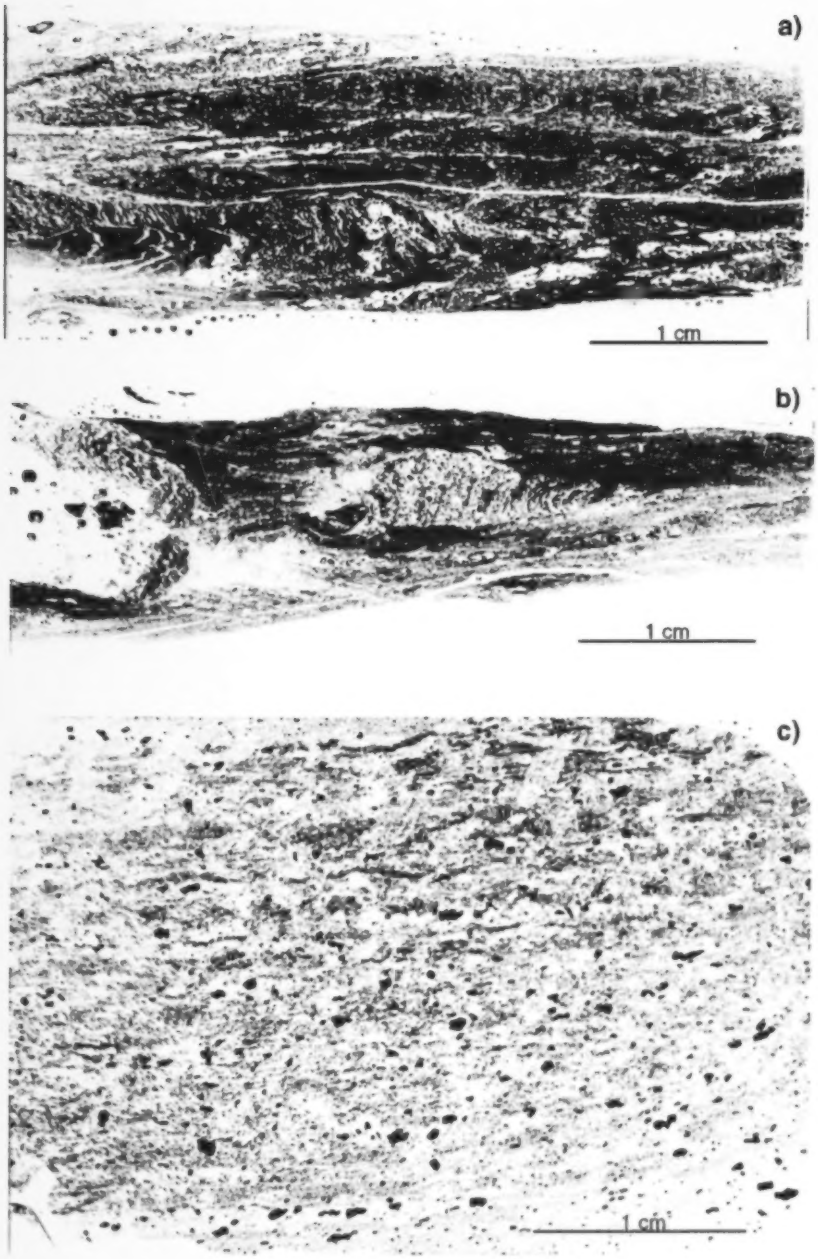

Figure 1. *Images of the polished thin sections for samples* ***a)*** *BAF-1,* ***b)*** *BAF-2, and* ***c)*** *BAF-AB. Folding and deformation are evident in 1a and 1b and the dark grains in 1c are pyrite.*

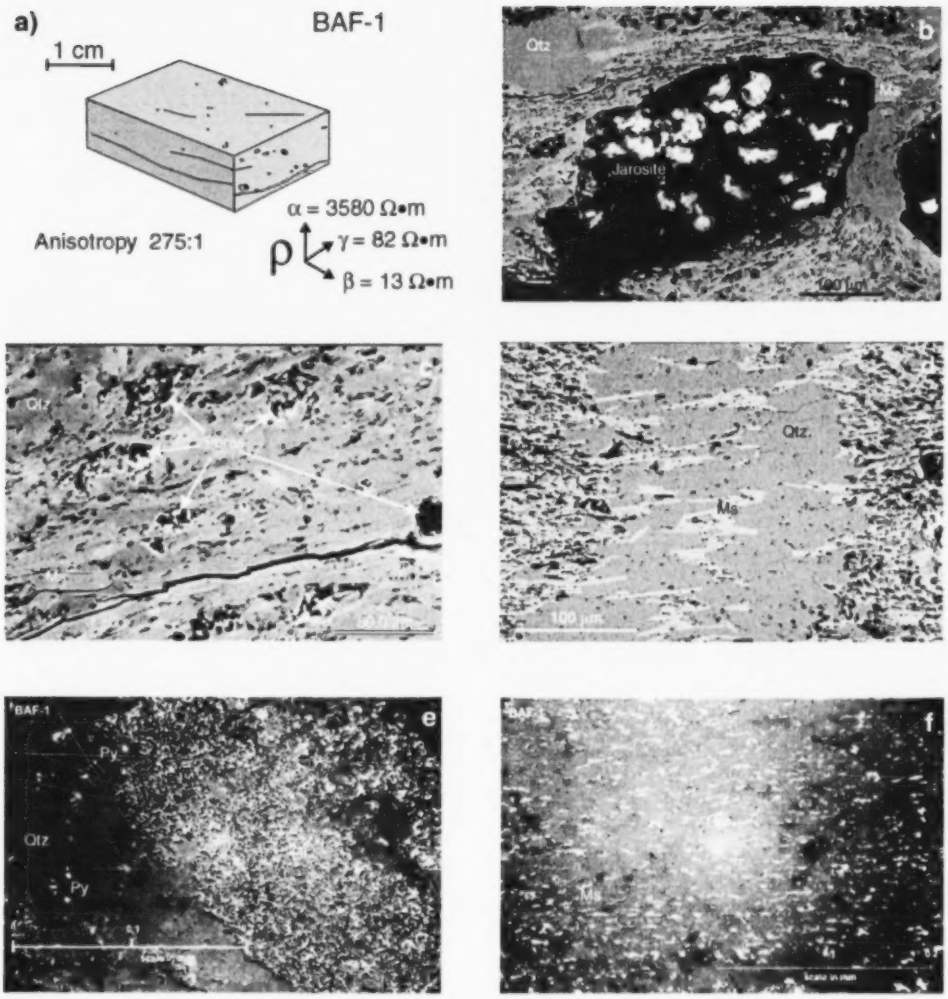

Figure 2. *Schematic presentation of a graphitic shale sample BAF-1 represented by* ***a)*** *a block diagram with sketches of the rock texture and 3-D electrical resistivity (ρ_r) values shown below. The scanning electron microscope images (SEM; backscattered electron image, BSE; and secondary electron image, SEI) show the orientation and distribution of the jarosite crystals, muscovite (lighter grey mineral), quartz (dark grey), and graphite. The SEM images are displayed for surfaces perpendicular to foliation (β- or γ-direction) highlighting* ***b)*** *jarosite crystals (BSE),* ***c)*** *distribution of pores (SEI), and a* ***d)*** *quartz vein crosscutting foliation (BSE). Reflected light images show* ***e)*** *intergrowth of graphite-rich lenses (white) and quartz-rich lenses (grey) in fold nose, and* ***f)*** *disseminated graphite flakes in a muscovite-rich layer (grey) elongated parallel to foliation. Ms, muscovite; Qtz, quartz; Gr, graphite; Py, pyrite.*

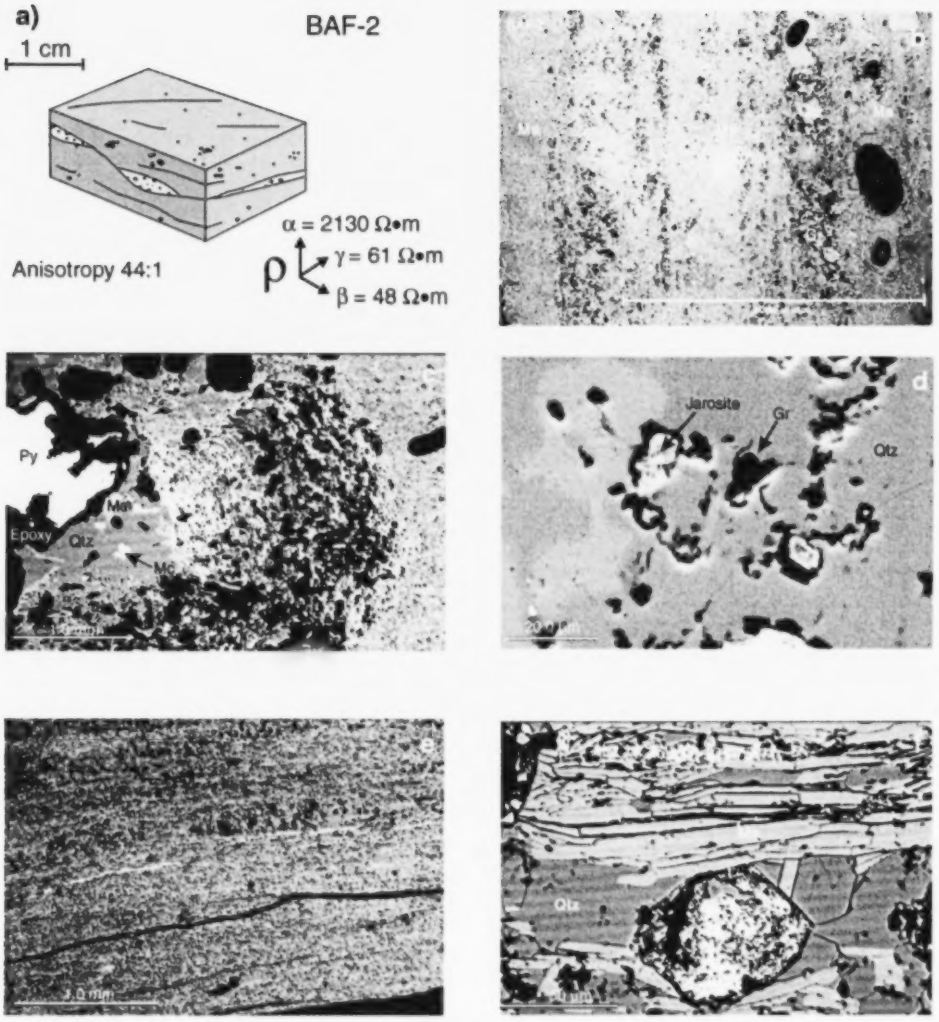

Figure 3. *Schematic presentations of graphitic shale sample BAF-2 represented by* **a)** *block diagram with sketches of the rock texture and 3-D ρ_r values shown below. Scanning electron microscope images displayed for surfaces perpendicular to foliation (β- or γ-direction) highlighting the* **b)** *reflected light image showing muscovite-rich layers alternating with quartz-rich layers. The graphite forms disseminated flakes parallel to foliation in the muscovite-rich layers and forms single grains and clots of slightly coarser grains in the quartz-rich layers. Mineralogy and orientation of grains are displayed in the BSE image;* **c)** *jarosite crystals are shown in the SEI image* **d)**; *BSE images* **e)** *and* **f)** *show the fine-grained sulphide-rich layers appearing to infill cracks and pores. Minerals identified on the images include pyrite (Py), quartz (Qtz), graphite (Gr), microcline (Mc), and muscovite (Ms).*

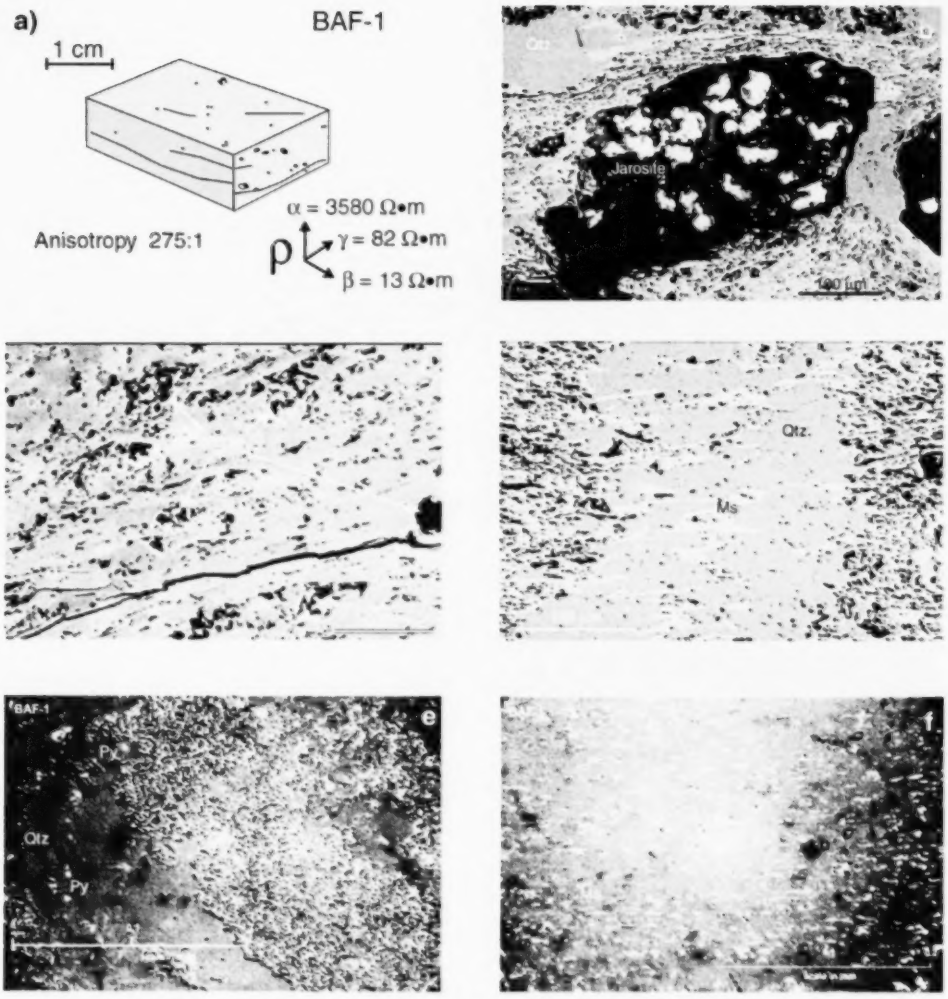

Figure 2. *Schematic presentation of a graphitic shale sample BAF-1 represented by* ***a)*** *a block diagram with sketches of the rock texture and 3-D electrical resistivity (ρ_a) values shown below. The scanning electron microscope images (SEM; backscattered electron image, BSE; and secondary electron image, SEI) show the orientation and distribution of the jarosite crystals, muscovite (lighter grey mineral), quartz (dark grey), and graphite. The SEM images are displayed for surfaces perpendicular to foliation (β- or γ-direction) highlighting* ***b)*** *jarosite crystals (BSE),* ***c)*** *distribution of pores (SEI), and a* ***d)*** *quartz vein crosscutting foliation (BSE). Reflected light images show* ***e)*** *intergrowth of graphite-rich lenses (white) and quartz-rich lenses (grey) in fold nose, and* ***f)*** *disseminated graphite flakes in a muscovite-rich layer (grey) elongated parallel to foliation. Ms, muscovite; Qtz, quartz; Gr, graphite; Py, pyrite.*

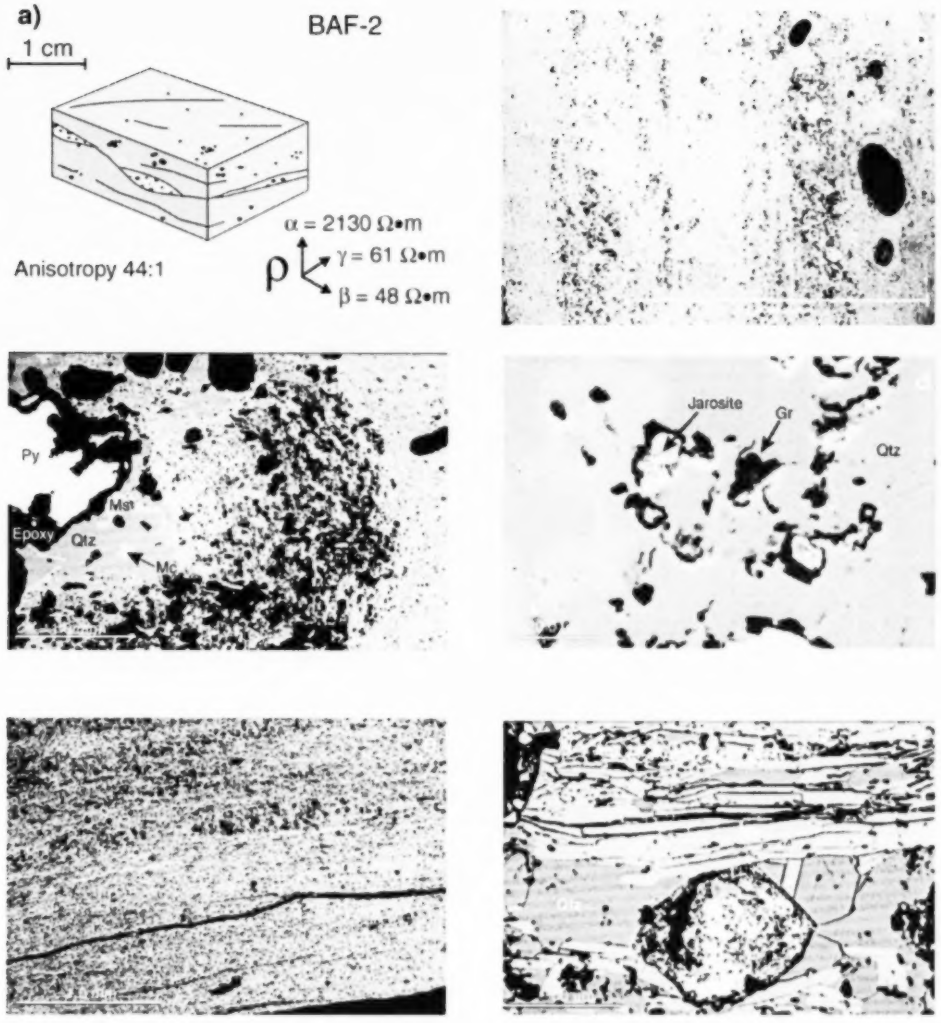

Figure 3. *Schematic presentations of graphitic shale sample BAF-2 represented by* ***a)*** *block diagram with sketches of the rock texture and 3-D ρ_r values shown below. Scanning electron microscope images displayed for surfaces perpendicular to foliation (β- or γ-direction) highlighting the* ***b)*** *reflected light image showing muscovite-rich layers alternating with quartz-rich layers. The graphite forms disseminated flakes parallel to foliation in the muscovite-rich layers and forms single grains and clots of slightly coarser grains in the quartz-rich layers. Mineralogy and orientation of grains are displayed in the BSE image;* ***c)*** *jarosite crystals are shown in the SEI image* ***d)****. BSE images* ***e)*** *and* ***f)*** *show the fine-grained sulphide-rich layers appearing to infill cracks and pores. Minerals identified on the images include pyrite (Py), quartz (Qtz), graphite (Gr), microcline (Mc), and muscovite (Ms).*

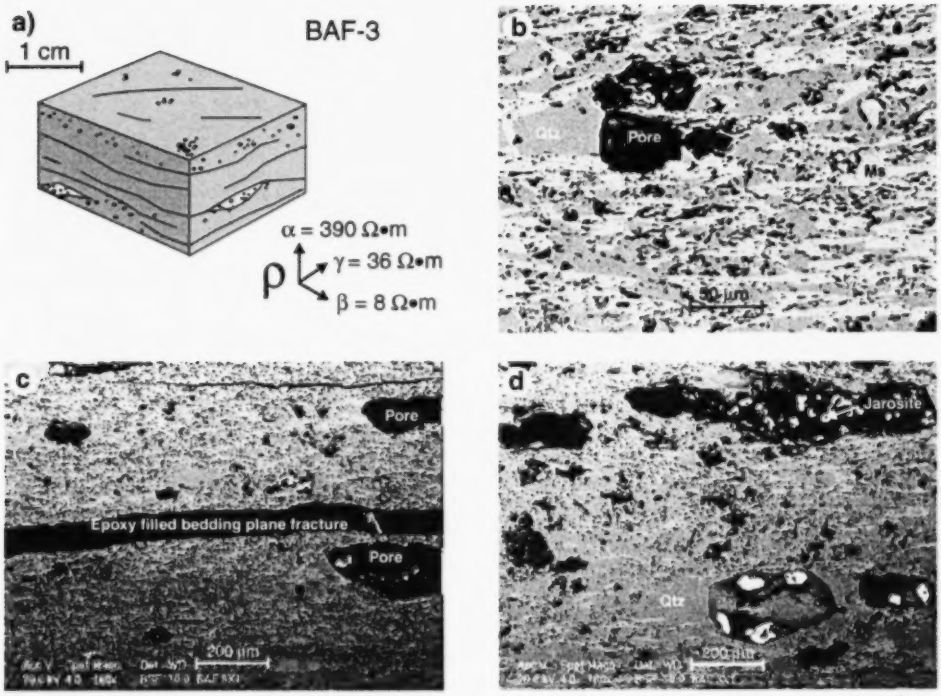

Figure 4. *Schematic presentations of graphitic shale sample BAF-3 represented by* ***a)*** *block diagram with sketches of the rock texture and 3-D ρ_r values shown below. The BSE images are displayed for surfaces perpendicular to foliation (β- or γ-direction) highlighting the* ***b)*** *distribution and parallel alignment of platy minerals,* ***c)*** *distribution of large pores, and* ***d)*** *large pore filled with jarosite. The SEM images show jarosite crystals (bright white) and distribution and orientation of pores (black), muscovite (Ms: light grey), and quartz (Qtz: dark grey).*

A schematic presentation of the graphitic shale sample BAF-1 is depicted in Figure 2a. The directions of the bulk electrical resistivities (ρ_r) are shown below the block diagram with 13–82 Ω•m in the directions parallel to foliation and 3580 Ω•m perpendicular to foliation. The electrical resistivity anisotropy (λ) for this sample is 275:1.The anisotropy is the ratio of the highest and lowest ρ_r values for samples when measured in three directions (Katsube et al., 1997b). Usually the direction parallel to foliation has the lowest ρ_r values and perpendicular to foliation has the highest ρ_r value. The specimen BAF-1x1 was polished for the SEM analysis on a surface perpendicular to foliation. This specimen has the highest anisotropy of the four samples analyzed and the highest storage porosity (12.87%, Connell-Madore et al. (2004)). Storage porosity (ϕ_S) is a function of the residual porosity ratio, ϕ_r, and the effective porosity, ϕ_E . Its calculation is based on data gained through mercury porosimetry analysis. Further details of the procedure are described elsewhere (Katsube et al., 1997a, 1998b). The storage pores (up to 150 by 600 µm for this sample) are predominantly oriented parallel to foliation and are partially infilled with jarosite crystals (Fig. 2b, c). A few of the cavities probably represent pyrite removed during weathering, as some have subhedral to euhedral cubic outlines. This sample is a strongly deformed layered schist. Deformation consists of microscopic shear folds on the scale of a few millimetres to a few centimetres which are visible on the thin section (Fig. 1a). The muscovite grains in this sample are all well aligned parallel to foliation and are likely contributing to the low ρ_r in the β- and γ-directions along with well connected grain-boundary pores and bedding-plane fractures (Fig. 2c, d). Graphite occurs mainly as flakes in the muscovite layers oriented parallel to foliation and is also concentrated in fold hinges. In one main quartz-graphite layer, graphite is concentrated strongly in bands that are intergrown with bands containing over 95% quartz. These bands are in part parallel to the original bedding and are best preserved in the fold nose. An example of a quartz vein crosscutting the foliation is shown in Figure 2d. These graphite and quartz bands are likely the primary contributors of the electrical mechanism of this sample. The presence of graphite (Fig. 2e, f) explains the low ρ_r parallel to foliation, given the poor connectivity between any sulphide grains or other highly conductive mineral grains. The higher ρ_r in the direction perpendicular to foliation is due to the quartz bands which would insulate and prohibit the flow of the electrical current in that direction.

A schematic presentation of graphitic shale sample BAF-2 is displayed in Figure 3a. The directions of ρ_r are shown below the block diagram with 48–61 Ω•m in the directions parallel to foliation and 2130 Ω•m perpendicular to foliation. The λ for this sample is 44:1. A polished thin section of

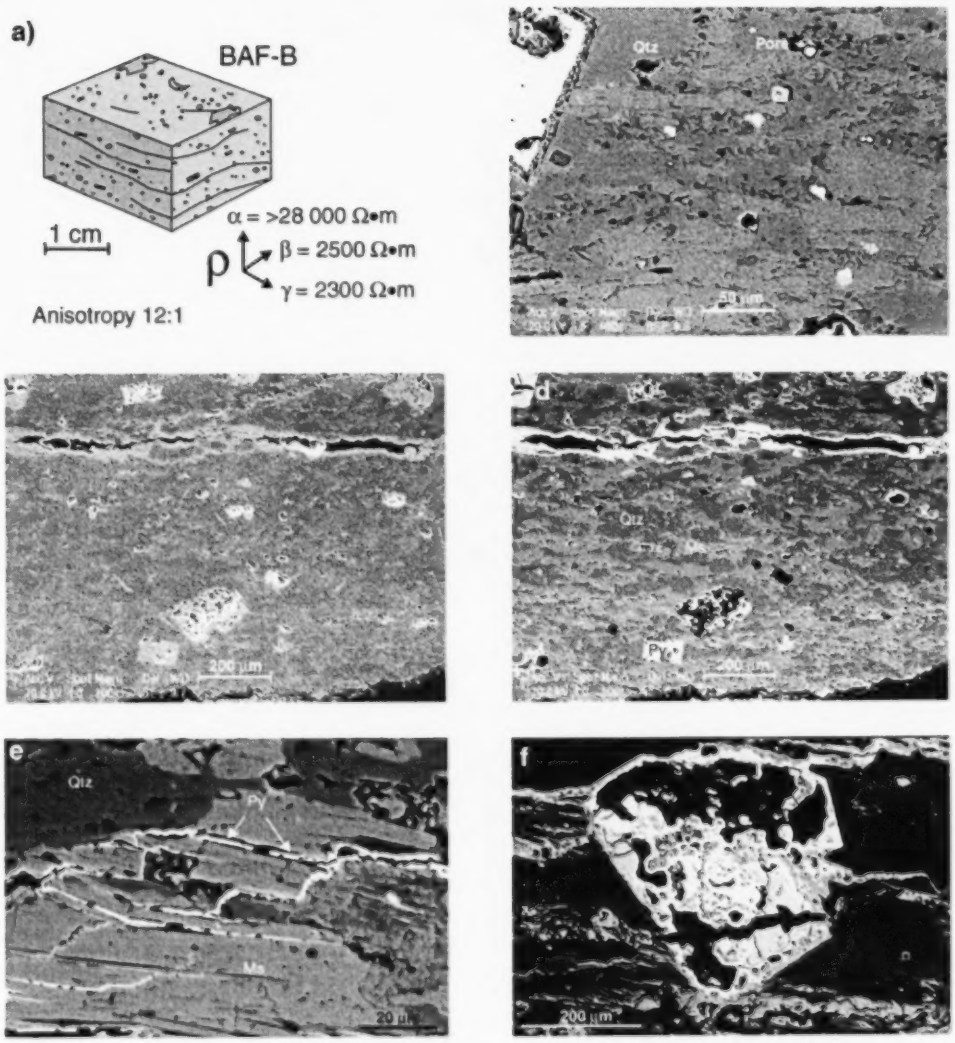

Figure 5. *Schematic presentation of graphitic shale sample BAF-B represented by* ***a)*** *block diagram with sketches of the rock texture and 3-D ρ_r values shown below.* ***b), c), d)*** *The SEM images are displayed for surfaces perpendicular to foliation (β- or γ-direction) highlighting the distribution and orientation of pores, quartz, and muscovite. The SEM images show pyritic alteration halo around a bedding-plane fracture (SEI) in Figure 5c, and in Figure 5d, the same in BSE.* ***e)*** *Pyrite stringers along muscovite grain boundaries (BSE).* ***f)*** *Highly altered pyrite grain showing preferential leeching of impurities and K-rich zones (BSE). The SEM images (BSE) show the foliation, and distribution of sulphide and other minerals identified (pyrite (Py), muscovite (Ms: light grey), and quartz (Qtz: dark grey)). The pore spaces are black.*

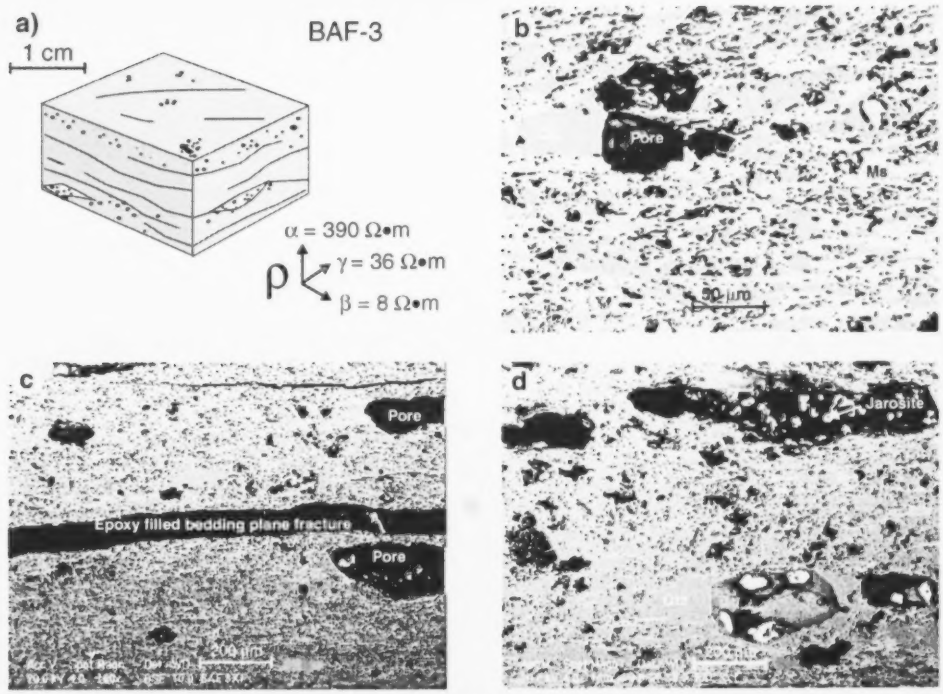

Figure 4. *Schematic presentations of graphitic shale sample BAF-3 represented by* ***a)*** *block diagram with sketches of the rock texture and 3-D ρ_r values shown below. The BSE images are displayed for surfaces perpendicular to foliation (β- or γ-direction) highlighting the* ***b)*** *distribution and parallel alignment of platy minerals,* ***c)*** *distribution of large pores, and* ***d)*** *large pore filled with jarosite. The SEM images show jarosite crystals (bright white) and distribution and orientation of pores (black), muscovite (Ms: light grey), and quartz (Qtz: dark grey).*

A schematic presentation of the graphitic shale sample BAF-1 is depicted in Figure 2a. The directions of the bulk electrical resistivities (ρ_r) are shown below the block diagram with 13–82 Ω•m in the directions parallel to foliation and 3580 Ω•m perpendicular to foliation. The electrical resistivity anisotropy (λ) for this sample is 275:1.The anisotropy is the ratio of the highest and lowest ρ_r values for samples when measured in three directions (Katsube et al., 1997b). Usually the direction parallel to foliation has the lowest ρ_r values and perpendicular to foliation has the highest ρ_r value. The specimen BAF-1x1 was polished for the SEM analysis on a surface perpendicular to foliation. This specimen has the highest anisotropy of the four samples analyzed and the highest storage porosity (12.87%, Connell-Madore et al. (2004)). Storage porosity (ϕ_S) is a function of the residual porosity ratio, ϕ_{rr}, and the effective porosity, ϕ_E . Its calculation is based on data gained through mercury porosimetry analysis. Further details of the procedure are described elsewhere (Katsube et al., 1997a, 1998b). The storage pores (up to 150 by 600 µm for this sample) are predominantly oriented parallel to foliation and are partially infilled with jarosite crystals (Fig. 2b, c). A few of the cavities probably represent pyrite removed during weathering, as some have subhedral to euhedral cubic outlines. This sample is a strongly deformed layered schist. Deformation consists of microscopic shear folds on the scale of a few millimetres to a few centimetres which are visible on the thin section (Fig. 1a). The muscovite grains in this sample are all well aligned parallel to foliation and are likely contributing to the low ρ_r in the β- and γ-directions along with well connected grain-boundary pores and bedding-plane fractures (Fig. 2c, d). Graphite occurs mainly as flakes in the muscovite layers oriented parallel to foliation and is also concentrated in fold hinges. In one main quartz-graphite layer, graphite is concentrated strongly in bands that are intergrown with bands containing over 95% quartz. These bands are in part parallel to the original bedding and are best preserved in the fold nose. An example of a quartz vein crosscutting the foliation is shown in Figure 2d. These graphite and quartz bands are likely the primary contributors of the electrical mechanism of this sample. The presence of graphite (Fig. 2e, f) explains the low ρ_r parallel to foliation, given the poor connectivity between any sulphide grains or other highly conductive mineral grains. The higher ρ_r in the direction perpendicular to foliation is due to the quartz bands which would insulate and prohibit the flow of the electrical current in that direction.

A schematic presentation of graphitic shale sample BAF-2 is displayed in Figure 3a. The directions of ρ_r are shown below the block diagram with 48–61 Ω•m in the directions parallel to foliation and 2130 Ω•m perpendicular to foliation. The λ for this sample is 44:1. A polished thin section of

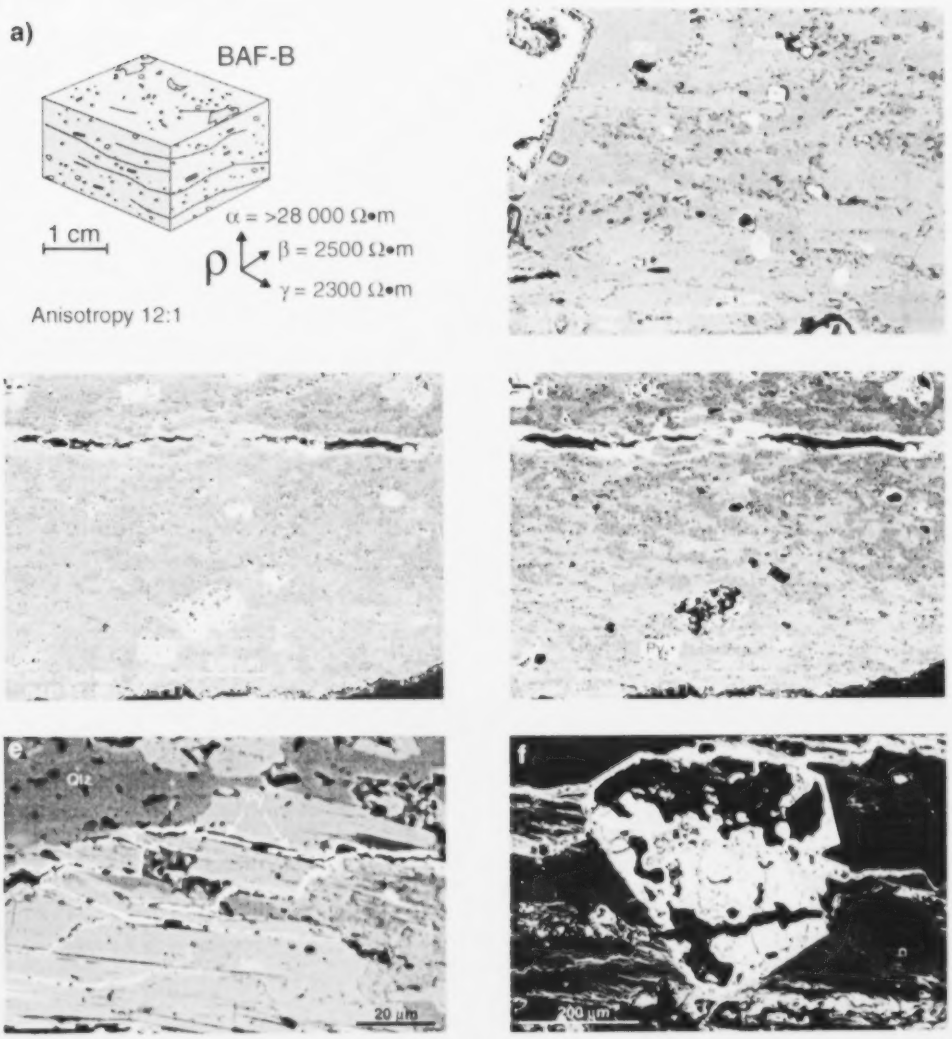

Figure 5. *Schematic presentation of graphitic shale sample BAF-B represented by* ***a)*** *block diagram with sketches of the rock texture and 3-D ρ_t values shown below.* ***b), c), d)*** *The SEM images are displayed for surfaces perpendicular to foliation (β- or γ-direction) highlighting the distribution and orientation of pores, quartz, and muscovite. The SEM images show pyritic alteration halo around a bedding-plane fracture (SEI) in Figure 5c, and in Figure 5d, the same in BSE.* ***e)*** *Pyrite stringers along muscovite grain boundaries (BSE).* ***f)*** *Highly altered pyrite grain showing preferential leeching of impurities and K-rich zones (BSE). The SEM images (BSE) show the foliation, and distribution of sulphide and other minerals identified (pyrite (Py), muscovite (Ms - light grey), and quartz (Qtz - dark grey)). The pore spaces are black.*

specimen BAF-2x1 was analyzed under the SEM. This specimen contained less quartz and graphite than specimen BAF-1x1, which would account for the slightly higher ρ_r values parallel to foliation and the lower ρ_r value perpendicular to foliation. Fine compositional banding is illustrated in Figure 3b. Quartz--graphite bands are interlayered with muscovite-graphite bands. The graphite is coarser grained and more irregular in shape in the quartz-rich layers than in the muscovite-rich layers. This sample also has a few interstitial patches of up to 0.5 mm, cryptocrystalline, light orange jarosite which was likely formed by the iron released by the weathering of the pyrite (Fig. 3d); however, the pores in this sample are not as large as those seen in samples BAF-1 and BAF-3, probably an indication of less weathering. There is approximately 0.3% pyrite and trace amounts of pyrrhotite and chalcopyrite present in this section. Subhedral outlines are observed in the replacement patches and are probably casts of pyrite grains. Light coloured bands visible in Figures 3e and 3f are difficult to explain. They are very fine grained consisting of galena, pyrite, quartz, and other minerals. These bands are fairly continuous, parallel to foliation, and also seem to infill some of the larger pores as seen in Figure 3f. Since not all pore spaces are filled with this material, it is believed to have developed in situ, and not as a result of the sample preparation. The electrical mechanism for this sample is likely the graphite and muscovite layers which increase electrical conductivity parallel to foliation. Muscovite layers could imply good pore interconnectivity in this direction. The sulphide minerals would have little effect on conductivity due to their poor connectivity and, in addition, some have corroded grain surfaces. One layer was noted to be dominated by quartz with only 20% muscovite. Layers such as these likely interrupt the electrical current flow in the direction perpendicular to foliation.

A schematic presentation of sample BAF-3 is displayed in Figure 4a. The directions of ρ_r are shown below the block diagram with 8–36 Ω•m in the directions parallel to foliation and 390 Ω•m perpendicular to foliation. The λ for this sample is 49:1. The subsample BAF-3x1 was polished for SEM analysis. There was not a polished thin section made for this sample. The platy minerals (muscovite) are all aligned parallel to foliation (Fig. 4b) which is likely contributing to the low ρ_r value in the β- and γ-directions. The electrical mechanisms are likely the connecting porosity along with the parallel alignment of platy minerals. Figures 4c and 4d appear very similar to those from sample BAF-1, although the ρ_r value in the direction perpendicular to foliation is considerably lower (390 Ω•m for BAF-3 and 3580 Ω•m for BAF-1). The reason for this difference is not known at present. This sample appears to be much less deformed than BAF-1 and BAF-2 which could be a contributing factor. Further investigation is required.

A schematic presentation of sample BAF-B is displayed in Figure 5a. The directions of ρ_r are shown below the block diagram, with 2300–2500 Ω•m in the directions parallel to foliation and over 28 000 Ω•m perpendicular to foliation. Specimen BAF-ABx1 was used for the SEM analysis. A surface perpendicular to foliation was polished for examination. Grain-boundary pores are visible in the SEM images (Fig. 5b) along with larger bedding-plane fracture pores that show evidence of alteration (K-rich halos in Fig. 5c, d). Fluid movement has likely occurred, creating the dissolution pores also visible in selected pyrite grains. There is no connectivity between the pyrite grains, although fluids have precipitated pyrite along muscovite cleavage planes (Fig. 4e). Figure 4f is a BSE image of an altered pyrite grain. The bright white is pyrite and the slightly darker areas are K-rich alteration. The platy minerals do not seem as abundant or well aligned as in the other samples. While the ϕ_E values for BAF-AB are considerably lower than BAF-1 and BAF-2, the connecting porosity (ϕ_c) value is comparable. This implies that although this sample lacks the larger storage pores that the others have, the connecting porosity is present. The alteration halos also support the good connectivity between pores. It is not understood why the ρ_r values are higher compared to the other samples examined even though this sample clearly has a higher sulphide content and well connected sulphide stringers along grain boundaries. The electrical mechanism for this sample is likely the pore spaces and sulphide stingers being obstructed by well connected quartz grains. Graphite is concentrated strongly in a few finer grained bands in which it forms scattered clusters of equant flakes and of more abundant slender, disseminated flakes. These are likely contributing to the lower ρ_r values parallel to foliation.

DISCUSSION AND CONCLUSIONS

The results of this study suggest that the anisotropic electrical resistivity characteristics are more likely determined by moderately good pore-fluid connectivity than well connected sulphide minerals. The two samples studied that have very low bulk electrical resistivity (ρ_r) values (Scromeda-Perez and Connell-Madore, 2004) parallel to foliation lack any significant mineralization, indicating the importance of a well developed foliation and connecting porosity system. The SEM analysis has confirmed that graphite is likely also a contributing factor. Sulphide minerals have had little to no effect on the electrical resistivity of these layers, for this set of samples. Well connected quartz grains form electrically insulating layers that interrupt the flow of electrical current, and result in the high ρ_r values (3580 Ω•m to more than 28 000 Ω•m) in the direction perpendicular to foliation.

These ρ_r values in the directions parallel and perpendicular to foliation are similar to those obtained for a mineralized carbonaceous sediment (Connell et al., 1999; Katsube et al, 1998a) with ρ_r values in the range of 12 Ω•m to 320 Ω•m.

ACKNOWLEDGMENTS

Samples were provided by A. Jones (GSC). The authors are grateful for the critical review of this paper and for the useful suggestions by T.J. Katsube (GSC). The authors would also like to thank A. Galley (GSC) for his comments and suggestions to the paper.

REFERENCES

Connell-Madore, S., Li, J., and Dexter, K.
2004 Pore-size distribution for graphitic shale samples from the Astarte River formation, Piling Group, Baffin Island, Nunavut; Geological Survey of Canada, Current Research 2004-C4.

Connell, S., Katsube, T.J., and Hunt, P.
1999 Textural characteristics of low to high resistivity sedimentary rocks, Bathurst mining camp, New Brunswick; *in* Current Research 1999-E, Geological Survey of Canada, p. 189–194.

Corrigan, D., Scott, D.J., and St-Onge, M.R.
2001 Geology of the northern margin of the Trans-Hudson Orogen (Foxe Fold Belt), central Baffin Island, Nunavut; Geological Survey of Canada, Current Research 2001-C23, 17 p.

Katsube, T.J., Dorsch, J., and Connell, S.
1997a Pore surface area characteristics of the Nolichucky Shale within the Oak Ridge Reservation (Tennessee, USA): implication for fluid expulsion efficiency; *in* Current Research 1997-E, Geological Survey of Canada, p. 117–124.

Katsube, T.J., Scromeda, N., Best, M.E., and Goodfellow, W.D.
1997b Electrical characteristics of mineralized and nonmineralized rocks at the Brunswick No. 12 deposit, Bathurst mining camp, New Brunswick; *in* Current Research 1997-E, Geological Survey of Canada, p. 97–107.

Katsube, T.J., Connell, S., Goodfellow, W., and Scromeda, N.,
1998a Electrical characteristics of nonmineralized rocks from the Bathurst mining camp, New Brunswick; *in* Current Research 1998-E, Geological Survey of Canada, p. 125–137.

Katsube, T.J., Cox, W.C., and Issler, D.R.
1998b Porosity characteristics of shale formations from the Western Canada Sedimentary Basin; *in* Current Research 1998-E, Geological Survey of Canada, p. 63–74.

Reed, S.J.B.
1997 Electron Microprobe Analysis, Cambridge University Press, Cambridge, United Kingdom, 346 p. (second edition).

Scromeda-Perez, N. and Connell-Madore, S.
2004 Electrical characteristics of rock samples from the central Baffin region, Baffin Island, Nunavut; Geological Survey of Canada, Current Research C-3.

Geological Survey of Canada Project Y14